Journal of Physics and Chemistry of Solids 86 (2015) 42–48

Contents lists available at ScienceDirect

Journal of Physics and Chemistry of Solids

journal homepage: www.elsevier.com/locate/jpcs

The cooperative Jahn–Teller effect and anti-isostructural phases in $Ni_{1-x}Co_xCr_2O_4$ solid solutions: Synchrotron X-ray diffraction study

A.S. Mikheykin [a,b,*], V.I. Torgashev [a], Yu.I. Yuzyuk [a], A.A. Bush [c], V.M. Talanov [d], A. Cervellino [e], V.P. Dmitriev [a,b]

[a] Faculty of Physics, Southern Federal University, 344090 Rostov-on-Don, Russia
[b] Swiss-Norwegian Beam Lines at ESRF, BP 220, 38043 Grenoble, France
[c] Moscow State Institute of Radio-Engineering, Electronics, and Automation (Technical University), 117464 Moscow, Russia
[d] The South Russia State Polytechnical University, Novocherkassk, Rostov Region 346428, Russia
[e] Swiss Light Source, Paul Scherrer Institute, CH-5232 Villigen, Switzerland

ARTICLE INFO

Article history:
Received 28 April 2015
Received in revised form
9 June 2015
Accepted 17 June 2015
Available online 18 June 2015

Keywords:
A. Ceramics
C. X-ray diffraction
D. Phase transitions
D. Crystal field
D. Crystal structure

ABSTRACT

A low-temperature high-resolution powder diffraction study has been carried out on a system of $Ni_{1-x}Co_xCr_2O_4$ solid solutions with $x \le 0.1$ down to 5 K. The tetragonal phase ($I4_1/amd$) with $c/a < 1$ was experimentally observed in $Ni_{0.9}Co_{0.1}Cr_2O_4$ below ~64 K. The new phase is anti-isostructural to the well-known tetragonal phase of $NiCr_2O_4$. A unified phenomenological model has been applied to structural phase transitions in $Ni_{1-x}Co_xCr_2O_4$ solid solutions. It shows that the appearing of such a phase is justified from a structural point of view. Analysis of atomic displacements confirms predictions of the symmetry-based model-free consideration.

1. Introduction

The complex oxides AB_2O_4 with spinel type structure, which contain *d* elements at the octahedral sites B, exhibit a broad diversity of physical properties. Such structures show complex magnetic phase diagrams; they are also superconductors, multiferroics, electrode materials, catalysts etc. In many cases their original properties relate to the structural peculiarity of spinels, which is the three-dimensional frustrated pyrochlore lattice formed by B-site ions. The existence of the large amount locally ordered or disordered spin, charge, orbital and atomic competing configurations possessing almost equal energies is one of the main features of such lattices [1–7].

In the chromium spinels ACr_2O_4 the Cr^{3+} ions are almost always occupy octahedral positions due to the high energy of the crystal field. Consequently, spinels are good model systems for the creation of solid solutions with ions substitution in the tetrahedral positions.

Frustration of spins at low temperature causes magnetic phase transitions (A = Mg: T_N = 12.5 K [8]; Zn: T_N = 12 K [9] or 12.7 K [10]; Cd: T_N = 7.8 K [11–13]; Hg: T_N = 5.8 K [14,15]) accompanied by structural tetragonal and orthorhombic distortions. Low temperature synchrotron X-ray [16] and neutron [10] diffraction studies revealed a tetragonal distorted structure for $MgCr_2O_4$ (space group $I4_1/amd$, a=5.89199(5) Å, c=8.31677(8) Å at 10 K). The corresponding structural transformation is very close or it even occurs simultaneously with magnetic phase transition. The low temperature high-resolution synchrotron X-ray diffraction data for $MgCr_2O_4$ and $ZnCr_2O_4$ showed co-existence of tetragonal $I4_1/amd$ and orthorhombic *Fddd* phases [17].

The physical behavior of the compounds is very complex and unusual for those spinels with magnetic ions in the tetrahedral A-positions. Examples of such spinels are $CoCr_2O_4$, $FeCr_2O_4$ and $MnCr_2O_4$. Frustration of the B-cation (pyrochlore) sublattice in these spinels leads to complex non-collinear magnetic structures with three magnetic sublattices: A, Cr_1 and Cr_2 [18]. The conical spin structure was observed in $CoCr_2O_4$, $FeCr_2O_4$ and $MnCr_2O_4$ at approximately T_s=27 K, T_s=35 K and T_s=14 K, respectively [1,19,20]. If A-cations are Jahn–Teller (JT) ions such as Cu^{2+} and Ni^{2+} in $CuCr_2O_4$ and $NiCr_2O_4$, as well as their solid solutions, then occurs the orbital degeneracy of electronic states, which can be lifted by cubic-to-tetragonal crystal structure distortions due cooperative JT effect. The magnetic geometrically frustrated system is

* Corresponding author at: Swiss-Norwegian Beam Lines at ESRF, CS40220, 38043 Grenoble, Cedex 9, France.
E-mail addresses: alexey.mikheykin@esrf.fr, aleksey.mikheykin@gmail.com (A.S. Mikheykin).

http://dx.doi.org/10.1016/j.jpcs.2015.06.015
0022-3697/

possible only for spinels with cubic structure, because the tetrahedron of the pyrochlore sublattice becomes irregular after JT tetragonal distortion. Thus the situation for cubic and tetragonal spinels may be significantly different in the vicinity of magnetic transition temperature. Nevertheless, simultaneous magnetic and structural phase transitions were observed in $CuCr_2O_4$ and $NiCr_2O_4$ tetragonal spinels [21]. A large amount of work shows the strong impact of the cooperative Jahn–Teller effect on the structure and properties of materials with not only the variation of temperature but external hydrostatic pressure [22–24].

In this paper, we study the structural phase transitions in a system of $Ni_{1-x}Co_xCr_2O_4$ solid solutions with the mixed JT and non-JT magnetic ions at tetrahedral A-positions of the normal spinel structure. The tuning off JT mechanism of the removing of orbital degeneracy by reducing the concentration of JT ions in solid solution leads to unexpected structural states.

The system calls the additional interest due to the recent discovery of the spontaneous polarization in $CoCr_2O_4$ [19,25–27] and, in some members of solid solutions family [28], with already existing magnetic order. Thus, these materials can be classified as multiferroics, which are of great interest from the viewpoint of thus various applications. This applies especially to the second type multiferroic with coupling between the magnetic ordering and the spontaneous polarization according to the classification given in Ref. [29].

In our paper we experimentally follow temperature-concentration evolution of the crystal distortion in $Ni_{1-x}Co_xCr_2O_4$ solid solutions down to 5 K. Then, we briefly introduce a unified phenomenological model which predicts the possible structural phase states, regardless of the microscopic mechanism of its implementation, and showing coherency of theoretical predictions and experimental results. Finally, we discuss structure aspects of the corresponding structural phase transitions induced by the 2D irreducible representation E_g.

2. Experimental

2.1. Sample preparation

The samples $Ni_{1-x}Co_xCr_2O_4$ with $x=0$, 0.005, 0.01, 0.015, 0.02, 0.1 were prepared following a standard solid state reaction procedure. The mixture of oxides, $(1-x)NiO{\cdot}xCoO{\cdot}Cr_2O_3$, was annealed at 1700 K for 3 h, then the pressurized cylindrical samples were annealed at 1850 K for 2 h. The resulting ceramic pellets were 10 mm in diameter and 2–3 mm thick. The sample composition was analyzed by energy dispersive spectroscopy. The average values for the composition of the spinel compounds were equal to the stoichiometry of oxides mixes with standard deviation less than 1 wt%.

2.2. X-ray diffraction

Temperature-dependent synchrotron X-ray powder diffraction data were collected at the BM01A beamline of the Swiss-Norwegian Beamlines, ESRF (Grenoble, France) using 2-D Pilatus2M (Dectris) detector. The temperature was changing in the ramp mode from 90 K to 300 K with typical step of 1.4 K by open-flow Oxford Cryostream700+ system. The monochromatic beam at wavelength $\lambda=0.682396$ Å was slitted down to $300\times300\ \mu m_2$. $200-\mu m-$ diameter glass capillaries were used for mounting finely grinded powder samples. The sample was rotated by 10 degrees. The sample-to-detector distance ($D\approx193$ mm), the tilt angles of the detector and the wavelength were calibrated using LaB_6 NIST standard. The calibration and subsequent integration were performed using fit2D software [30].

Low temperature high-resolution synchrotron radiation powder diffraction patterns were collected at the powder diffraction station of the Swiss Light Source – Materials Science beamline (SLS-MS) on the solid-state silicon microstrip 1-D detector MYTHEN at an incident photon energy of 20 keV ($\lambda=0.6204187$ Å). The sample was mounted in a Janis cryostat in 0.2 mm capillaries which spun at approximately 10 Hz during the 2θ scan to avoid preferred orientation and get better statistics. The sample-detector distance ($D\approx790$ mm) and the detector parameters were calibrated using a Silicon reference powder sample.

Rietveld refinement was carried out using FullProf suit [31]. The refined parameters were the scale factor, unit cell dimensions, atomic coordinates, isotropic displacement parameters, profile parameters. The pseudo-Voigt profile was employed for the refinement of data.

3. Results

The structural phase states of outer members of the family of solid solutions serve as a good reference as they are well known and presented in detail in many papers. The structure of $CoCr_2O_4$ is cubic (space group $Fd\bar{3}m$) up to 5 K [32]. $NiCr_2O_4$ undergoes two structural phase transformations with temperature decreasing. The first-order phase transition between the fcc (space group $Fd\bar{3}m$, Z=8) and fct (space group $I4_1/amd$, Z=4, $c/a>1$) structures is found to occur in the temperature range of 290–310 K. The second phase transition, between the tetragonal and orthorhombic phase, occurs at 70 K (see Refs. [21,33]). *Fddd* is a maximal nonisomorphic subgroup of $I4_1/amd$, which is derived from the parent $Fd\bar{3}m$ by loss of all three-fold rotation axes and part of the two-fold screw axes. In $NiCr_2O_4$, variable-temperature synchrotron x-ray diffraction measurements show additional structural changes below 30 K [21], in concurrence with anomalies in specific heat and susceptibility measurements of $NiCr_2O_4$ reported previously in the literature [34,21].

Diffraction data shows that the sample with $x=0.02$ contains about 1.3% admixture of NiO.

3.1. $Ni_{1-x}Co_xCr_2O_4$ with $x\le0.02$

A significant drop down of the first phase transition temperature occurs when substituting even small amount of the cobalt ions [35]. The structure of the solid solutions at room temperature is cubic when $x>0.005$. The second transition temperature is almost unchanged, for the crystals with small amount of substituted ions ($0\le x\le0.02$), while the phase transition to the orthorhombic phase, for the compound with $x=0.02$, occurs at 65 K. Fig. 1 (a) shows an example of the fit of the experimental profile by the Rietveld method. Figs. 1(b, c) shows a well resolved peak splitting as a result of the phase transition between the tetragonal and orthorhombic structures. Fig. 2 shows the temperature dependence of the lattice parameters and unit cell volume in the temperature range from 5 to 350 K.

3.2. $Ni_{1-x}Co_xCr_2O_4$ with $x=0.1$

At variance with above compounds the one with $x=0.1$ undergoes a phase transition from fcc to fct structure $I4_1/amd$ at $T=64$ K. However, the tetragonal phase in this sample has a ratio $c/a<1$, unlike the compounds with smaller x where $c/a>1$. Thus, there are two anti-isostructural phases with space group $I4_1/amd$.

Rietveld refinement fits of 20 K diffraction data to the tetragonal space group $I4_1/amd$ for $Ni_{0.9}Co_{0.1}Cr_2O_4$ is shown in Fig. 3(a). Symmetry lowering is demonstrated by the splitting of certain high symmetry diffraction peaks as shown in Fig. 3(b–c) for

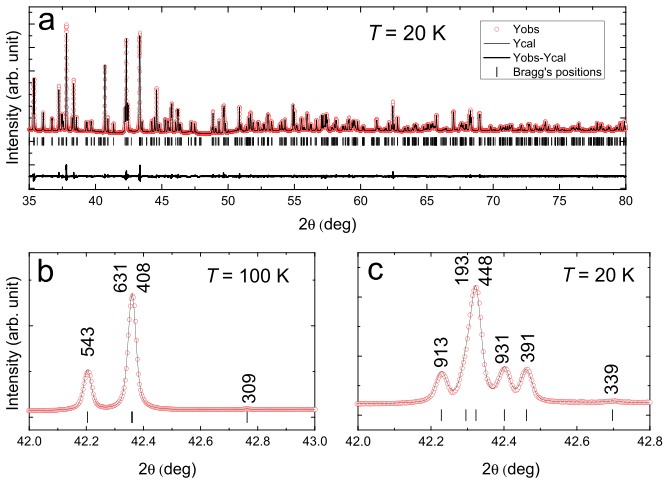

Fig. 1. High-resolution synchrotron x-ray powder diffraction pattern of $Ni_{0.995}Co_{0.005}Cr_2O_4$. (a) The low-temperature diffraction pattern of $Ni_{0.995}Co_{0.005}Cr_2O_4$ is indexed in the orthorhombic space group *Fddd*. The lowering of average crystal symmetry in $Ni_{0.995}Co_{0.005}Cr_2O_4$ from tetragonal to orthorhombic is illustrated by the splitting of the tetragonal reflections (b) into the orthorhombic reflections (c).

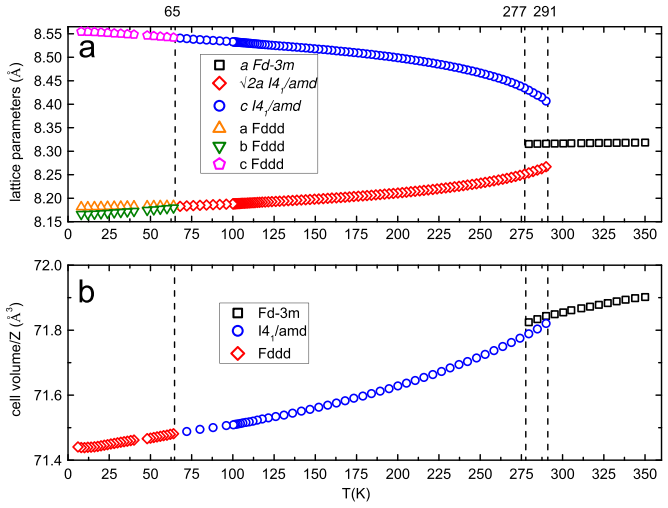

Fig. 2. Temperature evolution of the lattice parameters (a) and the cell volume (b) for $Ni_{0.995}Co_{0.005}Cr_2O_4$ solid solution. The values of the lattice parameter a for tetragonal phase ($I4_1/amd$) were multiplied by factor $\sqrt{2}$. Symbols represent experimental data. The cell volume normalized by the number of formula units (Z) in each cell shows a steady decrease with temperature. The vertical dash lines indicate the phase transitions temperature. The error bars are smaller than the symbol sizes in the both cases.

$Ni_{0.9}Co_{0.1}Cr_2O_4$. The changing of lattice parameters with temperature varying is illustrated in Fig. 4 for $Ni_{0.9}Co_{0.1}Cr_2O_4$.

The phase transitions from tetragonal to the orthorhombic phase for the sample with $x=0.1$ could not be identified, because peak splitting is very weak. The overall shape of the peaks at high angles becomes asymmetric but peaks are not resolved. It is worth noting that such structural transition is possible from the symmetry point of view. However, both presented temperature dependences show a deviation from the main trend at temperatures below 23 K.

A set of parameters derived from the Rietveld refinement procedure for all viewed phases is shown in Table 1.

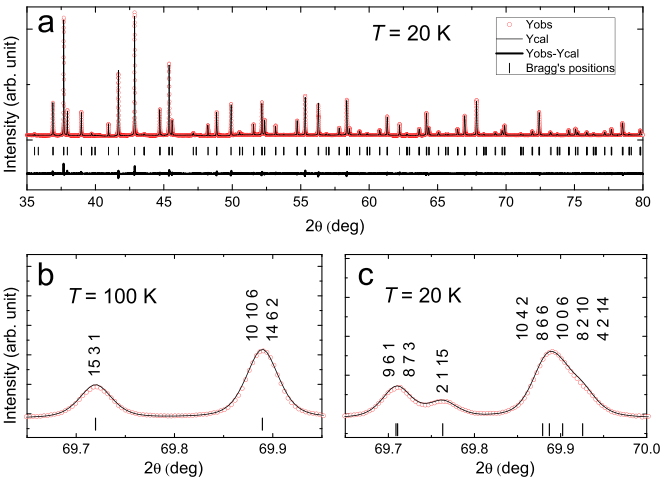

Fig. 3. High-resolution synchrotron x-ray powder diffraction of $Ni_{0.9}Co_{0.1}Cr_2O_4$. (a) The low-temperature diffraction pattern of $Ni_{0.9}Co_{0.1}Cr_2O_4$ is indexed in the tetragonal space group $I4_1/amd$. The lowering of average crystal symmetry in $Ni_{0.9}Co_{0.1}Cr_2O_4$ from cubic to tetragonal symmetry is illustrated by the splitting of the cubic reflections (b) into tetragonal reflections (c).

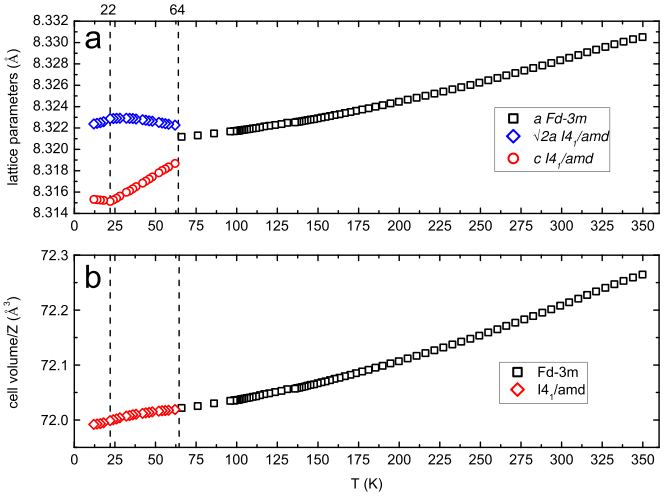

Fig. 4. Temperature evolution of the lattice parameters (a) and the cell volume (b) of the $Ni_{0.9}Co_{0.1}Cr_2O_4$ solid solution. The values of the lattice parameter a for tetragonal phase ($I4_1/amd$) were multiplied by factor $\sqrt{2}$. Symbols represent experimental data. The cell volume normalized by the number of formula units (Z) in each cell shows a steady decrease with temperature. The error bars are smaller than the symbol size in the both cases.

4. Discussion

4.1. Phenomenological model

In order to describe qualitatively the thermodynamic behavior of a system, the free energy is sufficient to be present as follows:

$$\Phi(P, T, \rho, \phi) = \Phi_0 + \alpha_1 I_1 + \beta_1 I_2 + \alpha_2 I_1^2 + \beta_2 I_2^2 + \delta I_1 I_2, \quad (1)$$

where are two polynomial invariants:

$$I_1 = \eta_1^2 + \eta_2^2, \quad (2)$$

$$I_2 = \eta_1^3 - 3\eta_1\eta_2^2. \quad (3)$$

The model based on the order-parameter expansion (1) has

Table 1
Structural parameters of $Ni_{0.995}Co_{0.005}Cr_2O_4$ and $Ni_{0.9}Co_{0.1}Cr_2O_4$ from Rietveld refinement at various temperatures.

Sample	$Ni_{0.995}Co_{0.005}Cr_2O_4$		$Ni_{0.9}Co_{0.1}Cr_2O_4$	
Crystal system	Cubic	Tetragonal	Orthorhombic	Cubic	Tetragonal
T (K)	350	100	20	350	20
Space group	$Fd\bar{3}m$ (N227)	$I4_1/amd$ (N141)	$Fddd$ (N70)	$Fd\bar{3}m$ (N227)	$I4_1/amd$ (N141)
origin	2	2	2	2	2
Z	8	4	8	8	4
a (Å)	8.31843(8)	5.78973(1)	8.18172(2)	8.33052(7)	5.884956(1)
b (Å)	8.31843(8)	5.78973(1)	8.16750(2)	8.33052(7)	5.884956(1)
c (Å)	8.31843(8)	8.53301(2)	8.55307(2)	8.33052(7)	8.315229(2)
Volume (Å^3)	575.604(17)	286.035(2)	571.552(4)	578.118(15)	287.9789(2)
Ni/Co	8b (3/8; 3/8; 3/8)	4b (0; 1/4; 3/8)	8a (1/8; 1/8 1/8)	8b (3/8; 3/8; 3/8)	4b (0; 1/4; 3/8)
B_{iso} (Å^2)	0.348(18)	0.1898(36)	0.2005(30)	0.401(14)	0.1708(23)
Cr	16c (0; 0; 0)	8c (0; 0; 0)	16d (1/2; 1/2; 1/2)	16c (0; 0; 0)	8c (0; 0; 0)
B_{iso} (Å^2)	0.229(16)	0.1382(33)	0.1675(25)	0.157(13)	0.1234(21)
O	32e (x; x; x) x=0.23747(25)	16h (0; y; z) y=0.51629(11) z=0.23272(6)	32h (x; y; z) x=0.25811(9) y=0.25784(9) z=0.26791(6)	32e (x; x; x) x=0.23754(19)	16h (0; y; z) y=0.52328(11) z=0.23816(10)
B_{iso} (Å^2)	0.554(46)	0.2341(64)	0.2883(58)	0.316(36)	0.2463(55)
R_p (%)	4.91	3.62	2.86	4.52	3.53

been comprehensively discussed in Refs. [36–38]. The symmetrized combinations of the diagonal components of the strain tensor can be considered as OP components η_1 and η_2 for observed proper ferroelastic transformations:

$$\eta_1 = \frac{1}{\sqrt{6}}(2e_3 - e_1 - e_2), \quad (4)$$

$$\eta_2 = \frac{1}{\sqrt{2}}(e_1 - e_2). \quad (5)$$

The experimentally measured strain can be found as

$$e_i = \frac{a_i}{a_0} - 1, \quad i = 1..3, \quad (6)$$

where a_i – lattice parameters a, b, c in pseudocubic representation; $a_0 = \sqrt[3]{abc}$ for the given temperature.

The equations of state result from the minimization of Φ with respect to the combinations of variables η_i.

The corresponding equations of state yield four possible equilibrium states:

0: $\eta_1 = \eta_2 = 0$ ($e_1 = e_2 = e_3 = 0$, $Fd\bar{3}m$, parent high-temperature phase);
I: $\eta_1 = \eta$ ($e_1 = e_2 > e_3$, $I4_1/amd$ with $c/a > 1$);
II: $\eta_2 = -\eta$ ($e_1 = e_2 < e_3$, $I4_1/amd$ with $c/a < 1$);
III: $\eta_1 \neq 0$, $\eta_2 \neq 0$, $\eta_1 \neq \eta_2$ ($Fddd$).

The model-free solutions 0–III are obtained solely from the analysis of the symmetry of the parent cubic phase. Hypothesis about the microscopic mechanism of the transitions were not been used, but the theory describes all experimentally observed phase. The versatility of this approach illustrates a similar situation in a completely different chemical systems of indium alloys [39].

4.2. Symmetry mode analysis

The structure distortions in low symmetry phases can be decomposed into contributions of different collective atomic shifts with symmetries defined by irreducible representations of the parent space group. It allows to distinguishing primary and secondary (induced) contributions with different symmetries. They contribute with various weights to the whole structure distortion. The symmetry-breaking distortion in a displacive type phase transition is mainly induced by the freezing of the primary phonon mode, related to the order parameter, and it is the basis of their treatment within the Landau theory.

The decomposition and estimation of the amplitudes for the symmetry frozen collective atomic shifts in distortion due displacive phase transition is a main objective of symmetry-mode analysis.

Three parameters are essential to point out a certain distortion symmetry unambiguously: a k-point, an irreducible representation (IR) and its order-parameter directions (OPD). Each distinct OPD vector will correspond to a different distortion.

We carried out decomposition and symmetry-mode analysis of the distortions using the online program ISODISPLACE [40]. Transformation matrix for tetragonal $I4_1/amd$ spinel structure from the parent cubic $Fd\bar{3}m$ phase can be represented as (1/2, −1/2, 0), (1/2, 1/2, 0), (0, 0, 1) with origin shift (3/4, 3/4, 0). For the cubic to orthorhombic structural transition: (1, 1, 0), (−1, 1, 0), (0, 0, 1), with origin shift (0, −3/2, 1/2). Results of the symmetry mode analysis are summarized in Table 2. Hereafter we use numbering of IRs and the corresponding reciprocal space vectors according to Kovalev's tables [41]. Also Miller and Love notation [42] is specified in parenthesis, because it is used in ISODISPLACE software. Fig. 5 graphically presents primary and secondary distortion modes for $NiCr_2O_4$ structure.

As one can see from Table 2, the active K-vector is $\mathbf{k}_{11}(0,0,0)$ for all transitions, which corresponds to the Γ-point at the Brillouin zone center. The spontaneous strain is associated with the Γ-point and, in the case of a proper ferroelastic transition, it is a primary order parameter. Total structure deformation consists of two components:

$$\varepsilon_{tot} = \varepsilon_{nsbr} + \varepsilon_{sbr},$$

where non-symmetry breaking ε_{nsbr} corresponds to the usual thermal expansion or contraction, and does not lead to structural phase transitions, and the second, critical symmetry breaking ε_{sbr} component is associated with the OP. The amplitudes of modes for transitions between the cubic and tetragonal phases in $Ni_{0.9}Co_{0.1}Cr_2O_4$ and $NiCr_2O_4$ have comparable magnitudes, and wherein the spontaneous deformations have the same sign, because the compression with decreasing temperature is present in all studied compounds.

Table 2
Normal modes for the structures $I4_1/amd$ and $Fddd$ of solid solutions $Ni_{1-x}Co_xCr_2O_4$ ($x=0.005$ and 0.1) with respect to parent phase $Fd\bar{3}m$. Primary modes are in bold. Modes given in Kovalev's [41] notation and notations of Miller and Love [42] (in parenthesis).

Sample	$Ni_{0.995}Co_{0.005}Cr_2O_4$						$Ni_{0.9}Co_{0.1}Cr_2O_4$	
Phase transition	$Fd\bar{3}m \rightarrow I4_1/amd$		$Fd\bar{3}m \rightarrow Fddd$		$I4_1/amd \rightarrow Fddd$		$Fd\bar{3}m \rightarrow I4_1/amd$	
k-point	$\mathbf{k}_{11}=0$							
IR	τ_1(GM1+)	τ_5(GM3 +)	τ_1(GM1+)	$\boldsymbol{\tau_5}$**(GM3 +)**	τ_1(GM1+)	τ_9(GM4 +)	τ_1(GM1+)	τ_5(GM3 +)
OPD	$\langle\xi\rangle$	$\langle\eta_1, 0\rangle$, $\eta_1=\eta$	$\langle\xi\rangle$	$\langle\eta_1, \eta_2\rangle$	$\langle\xi\rangle$	$\langle\zeta\rangle$	$\langle\xi\rangle$	$\langle\eta_1, 0\rangle$, $\eta_1=-\eta$
Isotropy subgroup	$Fd\bar{3}m$	$I4_1/amd$	$Fd\bar{3}m$	$Fddd$	$I4_1/amd$	$Fddd$	$Fd\bar{3}m$	$I4_1/amd$
Amplitudes (Å)	0.05461	0.17549	0.05067	0.19086 (η_1) −0.00449 (η_2)	−0.00557 −0.01521	0.00442	0.03074	0.00385
Strain	−0.00322	0.03387	−0.00367	0.03715 (η_1) 0.00121 (η_2)	−0.0023 0.00235	0.00123	−0.00216	−0.00072

By contrast, the amplitude of the primary modes τ_5(GM3+) differ by two orders of magnitude: amplitude is significantly greater for concentrated JT system $NiCr_2O_4$ than for $Ni_{0.9}Co_{0.1}Cr_2O_4$. Moreover, the primary mode amplitude of the displacements of the oxygen atoms in the spinel $NiCr_2O_4$ exceeds an order of magnitude of the non-symmetry breaking temperature compression one. This fact is one of the features of concentrated JT systems: increasing the unit cell parameters along certain crystallographic directions with decreasing temperature, or applying hydrostatic pressure. The corresponding spontaneous strains have a different sign, which related to the behavior of OP predicted for two anti-isostructural phases in the corresponding phenomenological model.

A similar situation occurs for solid solutions $Ni_{1-x}Cu_xCr_2O_4$ over temperature [43,44] and hydrostatic pressure changes [45]. Although in terms of the microscopic mechanism the situation in solid solutions of nickel and copper chromites is quite simple: the competing distortions involved in the cooperative Jahn–Teller effect give rise to two anti-isostructural phases. JT mechanism is dominant, and it completely suppresses possible effects of weak spin-orbit interaction in the structure. In solid solutions of nickel and cobalt chromites such a mechanism does not work due to the Jahn–Teller inactive cobalt ion in a tetrahedral surrounding. In the dilute JT system $Ni_{1-x}Co_xCr_2O_4$ there must be another mechanism for the stabilizing of the tetragonal phase $c/a < 1$.

Indeed, if a tetrahedron is compressed toward the xy plane, then we expect d_{xy} orbital to be higher in energy than d_{xz} and d_{yz} (Fig. 6). However, such deformation leads to E_g orbital degeneracy and becomes unstable. In that case the energy gain due to forming such distorted tetragonal structure with $c/a < 1$, must be higher than energy lost resulted from the degeneracy appearing. Further distortions can be expected due to the JT effect.

The origin of structural changes in $NiCr_2O_4$ is deformation of NiO_4 polyhedra. In a perfect tetrahedron all bond lengths are equal, and all angles are 109.47°. The ideal NiO_4 tetrahedra are observed in the cubic $NiCr_2O_4$ structure above 310 K, as well as in cubic $Ni_{1-x}Co_xCr_2O_4$ solid solutions with $x \leq 0.02$. Orbital ordering distorts tetrahedron so that a single Ni–O bond distance and two sets of O–Ni–O angles in the tetragonal phase. The Ni–O bond length is equal to 1.96239 Å, four angles O–Ni–O are 112.5045° and two angles O–Ni–O are 103.5614° for $Ni_{0.995}Co_{0.005}Cr_2O_4$ at 100 K. The orthorhombic structure preserves a single Ni–O bond length and three distinct pairs of O–Ni–O angles in the NiO_4 tetrahedra. For $Ni_{0.995}Co_{0.005}Cr_2O_4$ at 20 K, first pair of O–Ni–O angles is equal to 112.6453°, second is 112.9324°, and third is 103.0223°. Such kind of distortions in O–Ni–O bond angles result in an elongation of NiO_4 tetrahedra.

An analysis of the O–Ni–O angles in $Ni_{0.9}Co_{0.1}Cr_2O_4$ solid solution shows that the distortion angles also lead to elongating the tetrahedra along c-axis of unit cell, but much weaker than $NiCr_2O_4$. At 20 K in a solid solution two angles O–Ni–O are 109.44°, the remaining four are 109.4869°. The length of all bonds in the NiO_4 tetrahedron remains 1.97007 Å. This means that no anomalous energy configuration occurs (the right-hand side of Fig. 6) and there is no conflict with the expected JT effect. Table 3 compares distortions of tetrahedra and octahedra in anti-isostructural tetragonal phases with two indexes, which are both dimensionless and independent on size of polyhedron. The distortion index and quadratic elongation calculated as follows [46,47]

$$D = \frac{1}{n}\sum_{i=1}^{n}\frac{|l_i - l_{av}|}{l_{av}}, \tag{7}$$

$$\langle\lambda\rangle = \frac{1}{n}\sum_{i=1}^{n}\left(\frac{l_i}{l_0}\right)^2, \tag{8}$$

where D is a distortion index, l_i is the distance from central atom to ith coordinating atom, l_{av} is the average bond length, $\langle\lambda\rangle$ is quadratic elongation, l_0 is the center-to-vertex distance of a regular polyhedron of the same volume. For regular polyhedra in cubic phases the distortion index is 0 and quadratic elongation is 1.

From Table 3 it is clear that the distortions of the tetrahedra are negligible for tetragonal phase of $Ni_{0.9}Co_{0.1}Cr_2O_4$, whereas the distortion index of octahedra is three times higher than in the first sample with $c/a > 1$. That is strong evidence of the primary role playing by the oxygen octahedra distortion in the formation of the tetragonal phase with $c/a < 1$.

The IR E_g enters to the composition of a mechanical representation on Wyckoff positions 32(e) and octahedral tilt representation [48]. Therefore the chain of structural transitions $Fd\bar{3}m \leftrightarrow I4_1/amd \leftrightarrow Fddd$ is of the displacement type connected with octahedral tilt. For these reasons low-symmetry $I4_1/amd$ and $Fddd$ phases formed by octahedra tilting in the spinel structure [48]. Note the structural features of the tetragonal and orthorhombic structures of deformed spinel induced by rotation of the octahedral: the ordered arrangement of elongated (shortened) octahedra is not a "pure" ordering of the "ferro" type. The axes of elongated (shortened) octahedra and tetrahedra are parallel to each other in the case of "ferro"-type ordering (similar to parallel orientation of magnetic moments in ferromagnetics). The tilting of the octahedra leads to deviation from a parallel orientation of elongated (shortened) octahedral, more complex structure.

5. Conclusion and overlook

The unified phenomenological theory predicts for $Ni_{1-x}Co_xCr_2O_4$ solid solutions all the structural phases experimentally observed so far. The corresponding model justifies the anomalous elastic anisotropy by relating it to the spontaneous strain induced by a proper ferroelastic transition. However, the

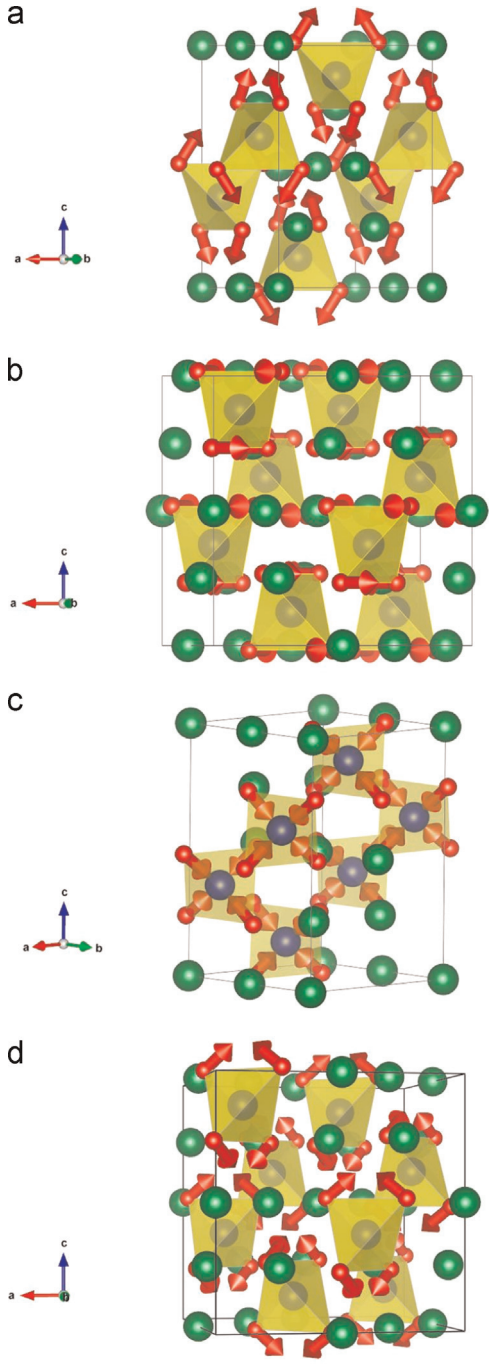

Fig. 5. The distortions corresponding to the IR $\langle \eta_1, 0 \rangle$ GM3+ (a) projected along the [0.5 1 0] direction with [0 0 1] upward vector; $\langle \eta_1, \eta_2 \rangle$ GM3+ (b) projected along the [0.2 1 0] direction with [0 0 1] upward vector; GM1+ for cubic to tetragonal transitions (c) projected along the [0.2 1 0] direction with [0 0 1] upward vector, and for tetragonal to orthorhombic transitions (d) projected along the [1 1 0] direction with [0 0 1] upward vector, in $NiCr_2O_4$. Ni and Co (blue) are tetrahedrally coordinated by oxygen (red). Chromium atoms are shown in green. The scale of the displacement vectors is arbitrary. (For interpretation of the references to color in this figure caption, the reader is referred to the web version of this paper.)

microscopic origin of appearance of tetragonal $c/a < 1$ phase is difficult to specify, because simultaneous acting of several mechanisms associated with different types of exchange and spin-orbital ordering is possible. However, when looking for a microscopic mechanism of the macroscopic elastic instability one should rely on the symmetry of the order parameter as a selection rule.

We investigated the structure of solid solutions with mixed JT and non-JT ions in tetrahedral positions, which show unusual

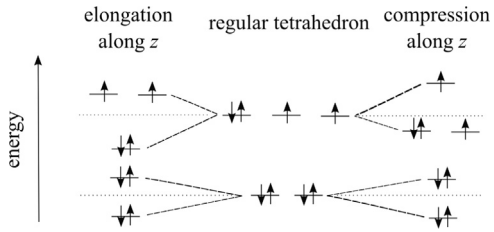

Fig. 6. Splitting of d energy levels for Ni^{2+} in regular tetrahedral surrounding of ligands with fully occupied e_g orbitals and partially occupied of t_{2g} orbitals (JT active case). Orbital splitting in the cases of further deformation are shown.

Table 3
Characterization of polyhedra distortion for two anti-isostructural tetragonal phases of $Ni_{1-x}Co_xCr_2O_4$ solid solutions.

Sample	D_{tetr}	$\langle\lambda\rangle_{tetr}$	D_{oct}	$\langle\lambda\rangle_{oct}$
$x=0.005$	0	1.0053	0.00026	1.0092
$x=0.1$	0	1	0.00078	1.0095

structural phase transitions. Certainly, the microscopic mechanism forming the new tetragonal phase cannot be determined solely on the basis of X-ray diffraction studies. Therefore, we call for additional works on neutron diffraction and magnetization measurements in order to determine the magnetic structure of solid solutions, and, for clarify, the role of magnetic ordering in the formation of the tetragonal $c/a < 1$ phase. Also the calorimetric measurements are needed as an independent determination of the temperatures of the magnetic and structural transitions, and their origin.

Acknowledgements

The authors acknowledge SLS for granting the beamtime. We thank as well SNBL for the opportunity of performing a part of synchrotron experiments. The research was partially supported by the Russian Foundation for Basic Research (Grant no. 13-02-12416 ofi m2). Some results of this work have been obtained with the support of the Ministry of Education and Science of the Russian Federation in the framework of the State task (Talanov V.M., project N2983(9.14)).

References

[1] K. Tomiyasu, J. Fukunaga, H. Suzuki, Phys. Rev. B 70 (2004) 1–12, http://dx.doi.org/10.1103/PhysRevB.70.214434.
[2] Y. Horibe, M. Shingu, K. Kurushima, H. Ishibashi, N. Ikeda, K. Kato, Y. Motome, N. Furukawa, S. Mori, T. Katsufuji, Phys. Rev. Lett. (2006), http://dx.doi.org/10.1103/PhysRevLett.96.086406.
[3] M. Iizumi, T.F. Koetzle, G. Shirane, S. Chikazumi, M. Matsui, S. Todo, Acta Crystallogr. Sect. B 38 (1982) 2121–2133, http://dx.doi.org/10.1107/S0567740882008176.
[4] J.P. Wright, P.G. Radaelli, Phys. Rev. B (2002), http://dx.doi.org/10.1103/PhysRevB.66.214422.
[5] I. Leonov, A.N. Yaresko, V.N. Antonov, M.A. Korotin, V.I. Anisimov, Phys. Rev. Lett. (2004), http://dx.doi.org/10.1103/PhysRevLett.93.146404 arXiv:0402363.
[6] G. Subías, J. García, J. Blasco, M.G. Proietti, H. Renevier, M.C. Sánchez, Phys. Rev. Lett. (2004), http://dx.doi.org/10.1103/PhysRevLett.93.156408.
[7] M. Schmidt, W. Ratcliff, P.G. Radaelli, K. Refson, N.M. Harrison, S.W. Cheong, Phys. Rev. Lett. 92 (2004) 056402, http://dx.doi.org/10.1103/PhysRevLett.92.056402 arXiv:0308101.
[8] S.H. Lee, C. Broholm, T.H. Kim, W. Ratcliff, S.-W. Cheong, Phys. Rev. Lett. (2000), http://dx.doi.org/10.1103/PhysRevLett.84.3718, URL: arXiv:9908433.
[9] I. Kagomiya, H. Sawa, K. Siratori, K. Kohn, M. Toki, Y. Hata, E. Kita, Ferroelectrics 268 (2002) 327–332, http://dx.doi.org/10.1080/00150190211050.
[10] L.W. Martin, S.P. Crane, Y.-H. Chu, M.B. Holcomb, M. Gajek, M. Huijben, C.-H. Yang, N. Balke, R. Ramesh, J. Phys. Condens. Matter 20 (2008) 434220, http://dx.doi.org/10.1088/0953-8984/20/43/434220.

[11] J.H. Chung, M. Matsuda, S.H. Lee, K. Kakurai, H. Ueda, T.J. Sato, H. Takagi, K. P. Hong, S. Park, Phys. Rev. Lett. (2005), http://dx.doi.org/10.1103/PhysRevLett.95.247204 arXiv:0510363.
[12] R. Valdés Aguilar, A.B. Sushkov, Y.J. Choi, S.W. Cheong, H.D. Drew, Phys. Rev. B 77 (2008) 92412, http://dx.doi.org/10.1103/PhysRevB.77.092412.
[13] M. Rovers, P. Kyriakou, H. Dabkowska, G. Luke, M. Larkin, A. Savici, Phys. Rev. B (2002), http://dx.doi.org/10.1103/PhysRevB.66.174434.
[14] H. Ueda, H. Mitamura, T. Goto, Y. Ueda, Phys. Rev. B (2006), http://dx.doi.org/10.1103/PhysRevB.73.094415.
[15] M. Matsuda, H. Ueda, A. Kikkawa, Y. Tanaka, K. Katsumata, Y. Narumi, T. Inami, Y. Ueda, S.H. Lee, Nat. Phys. 3 (2007) 397–400, http://dx.doi.org/10.1038/nphys586, URL: arXiv:0707.0280.
[16] H. Ehrenberg, M. Knapp, C. Baehtz, S. Klemme, Powder Diffr. 17 (2002) 230, http://dx.doi.org/10.1154/1.1479738, URL: ⟨http://journals.cambridge.org/abstract_S088571560000720X.
[17] M.C. Kemei, P.T. Barton, S.L. Moffitt, M.W. Gaultois, J.A. Kurzman, R. Seshadri, M.R. Suchomel, Y.-i. Kim, J. Phys. Condens. Matter 25 (2013) 1–5, http://dx.doi.org/10.1088/0953-8984/25/32/326001 arXiv:1302.5746v2.
[18] T.A. Kaplan, N. Menyuk, Philos. Mag. 87 (2007) 3711–3785, http://dx.doi.org/10.1080/14786430601080229.
[19] Y. Yamasaki, S. Miyasaka, Y. Kaneko, J.P. He, T. Arima, Y. Tokura, Phys. Rev. Lett. (2006), http://dx.doi.org/10.1103/PhysRevLett.96.207204.
[20] G. Shirane, D.E. Cox, S.J. Pickart, J. Appl. Phys. 35 (1964) 954–955, http://dx.doi.org/10.1063/1.1713556, URL: ⟨http://link.aip.org/link/JAPIAU/v35/i3/p954/s1&Agg=doi⟩.
[21] M.R. Suchomel, D.P. Shoemaker, L. Ribaud, M.C. Kemei, R. Seshadri, Phys. Rev. B 86 (2012) 054406, http://dx.doi.org/10.1103/PhysRevB.86.054406, URL: http://link.aps.org/doi/10.1103/PhysRevB.86.054406.
[22] I. Loa, P. Adler, A. Grzechnik, K. Syassen, U. Schwarz, M. Hanfland, G. K. Rozenberg, P. Gorodetsky, M.P. Pasternak, Phys. Rev. Lett. 87 (2001) 125501, http://dx.doi.org/10.1103/PhysRevLett.87.125501.
[23] J. Ruiz-Fuertes, A. Segura, F. Rodríguez, D. Errandonea, M.N. Sanz-Ortiz, Phys. Rev. Lett. (2012), http://dx.doi.org/10.1103/PhysRevLett.108.166402.
[24] M. Guennou, P. Bouvier, P. Toulemonde, C. Darie, C. Goujon, P. Bordet, M. Hanfland, J. Kreisel, Phys. Rev. Lett. (2014), http://dx.doi.org/10.1103/PhysRevLett.112.075501.
[25] Y.J. Choi, J. Okamoto, D.J. Huang, K.S. Chao, H.J. Lin, C.T. Chen, M. Van Veenendaal, T.A. Kaplan, S.W. Cheong, Phys. Rev. Lett. (2009), http://dx.doi.org/10.1103/PhysRevLett.102.067601.
[26] L.J. Chang, D.J. Huang, W.-H. Li, S.-W. Cheong, W. Ratcliff, J.W. Lynn, J. Phys. Condens. Matter 21 (2009) 456008, http://dx.doi.org/10.1088/0953-8984/21/45/456008.
[27] D. Kamenskyi, H. Engelkamp, T. Fischer, M. Uhlarz, J. Wosnitza, B.P. Gorshunov, G.a. Komandin, a.S. Prokhorov, M. Dressel, a.a. Bush, V.I. Torgashev, a.V. Pronin, Phys. Rev. B 87 (2013) 134423, http://dx.doi.org/10.1103/PhysRevB.87.134423, URL: http://link.aps.org/doi/10.1103/PhysRevB.87.134423.
[28] A.A. Bush, V.Y. Shkuratov, K.E. Kamentsev, A.S. Prokhorov, E.S. Zhukova, B. P. Gorshunov, V.I. Torgashev, Phys. Rev. B 85 (2012) 214112, http://dx.doi.org/10.1103/PhysRevB.85.214112.
[29] D. Khomskii, Physics 2 (2009) 20, http://dx.doi.org/10.1103/Physics.2.20, URL: http://link.aps.org/doi/10.1103/Physics.2.20.
[30] A. Hammersley, High Press. Res. 14 (1996) 235–248 , URL: http://www.tandfonline.com/doi/abs/10.1080/08957959608201408.
[31] J. Rodriguez-Carvajal, Int. Union Crystallogr. Newsl. December (2) (2001) 12–19.
[32] V. Tsurkan, S. Zherlitsyn, S. Yasin, V. Felea, Y. Skourski, J. Deisenhofer, H.-a. von Nidda, J. Wosnitza, A. Loidl, Phys. Rev. Lett. 110 (2013) 115502, http://dx.doi.org/10.1103/PhysRevLett.110.115502, URL: http://link.aps.org/doi/10.1103/PhysRevLett.110.115502.
[33] H. Ishibashi, T. Yasumi, J. Magn. Magn. Mater. 310 (2007) e610–e612, http://dx.doi.org/10.1016/j.jmmm.2006.10.1131, URL: ⟨http://www.sciencedirect.com/science/article/pii/S0304885306019639⟩.
[34] S. Klemme, J.C. Van Miltenburg, Phys. Chem. Miner. 29 (2002) 663–667, http://dx.doi.org/10.1007/s00269-002-0280-4.
[35] A.S. Mikheykin, D.Y. Chernyshov, A.A. Bush, A.S. Prokhorov, Y.I. Yuzyuk, V. P. Dmitriev, Phys. Solid State 56 (2014) 785–791, http://dx.doi.org/10.1134/S1063783414040209, URL: ⟨http://link.springer.com/10.1134/S1063783414040209.
[36] V.P. Sakhnenko, V.M. Talanov, Sov. Phys. Solid State 21 (1979) 34.
[37] A.A. Mukovnin, V.M. Talanov, Solid State Commun. 152 (2012) 2013–2017, http://dx.doi.org/10.1016/j.ssc.2012.08.015.
[38] V. Talanov, A. Mukovnin, Eur. Phys. J. B (2013), http://dx.doi.org/10.1140/epjb/e2013-40560-x.
[39] V. Dmitriev, D. Chernyshov, Y. Filinchuk, V. Degtyareva, Phys. Rev. B 75 (2007) 024111, http://dx.doi.org/10.1103/PhysRevB.75.024111, URL: http://link.aps.org/doi/10.1103/PhysRevB.75.024111.
[40] B.J. Campbell, H.T. Stokes, D.E. Tanner, D.M. Hatch, J. Appl. Crystallogr. 39 (2006) 607–614, http://dx.doi.org/10.1107/S0021889806014075, URL: ⟨http://scripts.iucr.org/cgi-bin/paper?S0021889806014075⟩.
[41] O. Kovalev, Irreducible Representations of the Space Groups, Russian Monographs and Texts on the Physical Sciences, Gordon and Breach, 1965, URL: ⟨http://books.google.ru/books?id=H1_hOZf3pRUC⟩.
[42] H.T. Stokes, D.M. Hatch, Isotropy Subgroups of the 230 Crystallographic Space Groups, 1988, URL: ⟨http://www.worldscibooks.com/physics/0751.html⟩. http:dx.doi.org/10.1142/0751.
[43] Y. Kino, S. Miyahara, J. Phys. Soc. Jpn. 21 (1966) 2732.
[44] M. Tovar, R. Torabi, C. Welker, F. Fleischer, Physica B Condens. Matter 385–386 (2006) 196–198, http://dx.doi.org/10.1016/j.physb.2006.05.181, URL: ⟨http://linkinghub.elsevier.com/retrieve/pii/S0921452606010751⟩.
[45] A.S. Mikheykin, V.I. Torgashev, V.M. Talanov, a.a. Bush, D. Chernyshov, I. Yu Yuzyuk, V.P. Dmitriev, J. Phys. Condens. Matter 26 (2014) 505401, http://dx.doi.org/10.1088/0953-8984/26/50/505401, URL: ⟨http://www.ncbi.nlm.nih.gov/pubmed/25407325⟩.
[46] W.H. Baur, The geometry of polyhedral distortions. Predictive Relationships for the Phosphate Group, 1974, http:dx.doi.org/10.1107/S0567740874004560.
[47] K. Robinson, G.V. Gibbs, P.H. Ribbe, Science 172 (1971) 567–570, http://dx.doi.org/10.1126/science.172.3983.567.
[48] V.M. Talanov, V.B. Shirokov, Acta Crystallogr. Sect. A 68 (2012) 595–606, http://dx.doi.org/10.1107/S0108767312028991.